The experimental determination of the relationship between stress, strain, acoustic velocity and density in greenwood *Pinus radiata*

Nicholas Davies, Clemens Altaner and Luis Apiolaza

January 11, 2015

New Zealand School of Forestry, University of Canterbury

Abstract

This paper presents a number of important constants needed for the use of mathematical modelling of greenwood *Pinus radiata*. The constants include all three necessary Youngs and shear moduli along with the six Poisson ratios needed for describing orthotropic materials in the elastic domain. Further yield surfaces and ultimate tensile strength are investigated. The accuracy of the various measurements are discussed in detail.

1 Introduction

While density and acoustic tests are common practice for obtaining dynamic modulus (which can in turn be used to estimate the static modulus (Barker, 1998; Lindstrm et al., 2004)) in both timber research and industry, little information about the underlying structure of wood is obtained from these tests. Wood is often dried to 6-12% moisture content before conducting any experimental work, which has been observed to alter the mechanical properties (Skaar, 1988; Ozyhar et al., 2013). Investigating dry wood gives a poor representation of the living organism, leaving scientists interested in the growth of trees somewhat in the dark when considering the way trees react to mechanical phenomenan. Unfortunately there is a lack of information on both green (the state of wood when it is inside a living tree) and core wood (wood produced by a young cambium).

Wind loading can cause mechanical failure which can decrease the value of processed timber due to defects, the associated financial loss has led to a substantial amount of research on predicting wind throw and wind damage risk for commercial species (Gardiner et al., 2008). However, these models do not investigate the structural failure within the tree, they only attempt to identify how likely failure is to occur in a particular environment. In areas with less pronounced prevailing wind directions there may be an effect on the stiffness of the trees in order to compensate for the multi-directional loadings (Apiolaza et al., 2011; Kern et al., 2005), this reduction in stiffness can result in a timber product of lower value.

One way of investigating mechanical phenomenon present in tree stems is the use of mathematical models, using the Finite Element Method (FEM). However because of the size of the tree, modelling an entire tree from the molecular level is infeasible, so homogenization is used. In order to use these methods experimental data is required to parametrize them. Full sets of constants even for dry timber are hard to find and to the best of our knowledge there are no full sets available for green or core wood radiata. Proportional limit and ultimate failure surfaces for all directions in green and core wood have also not been reported previously. Lack of available data is an issue for a number of current problems in plant biophysics.

The purpose of this paper is to present a number of necessary material constants for describing green core and outer wood as an orthotropic material. A set of static moduli and Poisson ratios for green core and outer wood in the radial, tangential and longitudinal (to the grain) directions. The small study was completed with *Pinus radiata* selected from plantations in Canterbury, New Zealand.

2 Experimental Method

2.1 Sample Selection and Preparation

Green radiata pine (*Pinus radiata*) samples were sourced from a sawmill in Canterbury, New Zealand. Four boards were chosen from approximately 30 boards to represent extremes of outerwood and corewood based on green density and dynamic modulus (Table 3). Green dynamic modulus was calculated from acoustic velocity measurements and green mass (Chauhan et al., 2013).

The samples were docked into approximately 500 mm lengths and stored in sealed bags with excess water at $5°C$ subsequently 6 defect-free, straight grained test specimens of the required shape and orientation were machined from each of the four boards and stored in sealed bags with excess water until testing. Prior to mechanical testing each specimen was weighed and it's volume measured by water displacement.

2.2 Testing

The specimens were placed into a Universal Testing Machine (UTM)(Instron 5566) set-up for the appropriate test. Displacement was tracked on the two faces perpendicular to the axis of loading with two digital cameras fitted with 60 mm micro lenses. Timelapse photography was used taking images every 3 seconds during the test, controlled via gphoto2 (Contributors, 2013).

For compression testing, samples approximately 15 x 15 x 30 mm were used with their grain oriented in longitudinal, radial or tangential direction. The UTM fitted with a x KN load cell having an accuracy of 0.1 N was run at a constant velocity of 1.5 mm per min for 300 seconds applying compression to the top of the sample.

Tension testing used bone shaped samples with dimensions approximately 50 x 25 x 6.5 mm with the breakage plane having an area of approximately 6.5 x 6.5 mm. With the exception of the longitudinal direction, where a straight stick test was used.

For the shear plane L shaped samples with a shear plane approximately 15 x 15 mm was used.

Once the specimens had been mechanically tested they were oven dried at $104°C$ until a representative sample was no longer losing weight 48 hours apart. Each sample was weighted and volume measured using the displacement method. From one specimen of each sample and test (ie 12 in total) a small strip approximately 1 x 5 x 10 mm was taken for x-ray diffraction testing. The micro-fibril angle and standard deviation of the micro-fibrils were obtained using the methods described in Cave and Robinson (1998b) and Cave and Robinson (1998a).

The time and load applied was extracted from the UTM data for use with the photo collections to create stress strain curves. This was implemented using Digital Image Correlation and Tracking with Matlab scripts (Chris Eberl, 06) to track identifiable points within the photos throughout each series to obtain

strain versus photo number curves. The time of each photo was obtained from the EXIF data attached to the photo obtained from the Python Imaging Library (Lundh et al., 95) and used to match the corresponding load applied by the UTM along with the dimension measurements which are used to calculate the stress strain curves.

During the process of extracting strain information from the images, a visual inspection of the data was undertaken. This involved using displacement versus image number, displacement vs neighbour's displacement and area of interest selection (available from Chris Eberl (06)) to determine the points which have been tracked correctly within the photo series. One-Dimensional average strains are taken in both the vertical and horizontal direction.

Because the UTM runs at a set velocity it is possible to estimate the strain on the sample, although this tends to slightly overestimate the strain. Initially there is a period of motion before the compression plate comes into contact and re orientates the sample, (although this is minimal) providing a good estimation to select the accuracy tracked points. The horizontal direction within the photographs is used to track the displacement perpendicular to the applied load. Here the assumption is made that points tracked accuracy in the vertical direction are tracked reliably in the horizontal direction.

2.3 Calculation of the Elastic Modulus

For each test of each specimen a visual inspection of the stress strain curves is undertaken, the initial reorientation of the sample, resulting in a curve before the linear elastic region is discarded, and the linear portion of the stress strain curve identified by overlaying a linear model $y = mx$ to the data being considered. Once there was as little deviation between the data and model as possible, this was considered the elastic region with the Elastic modulus E being the gradient m of the model. The end point of the fitted model is considered the limit of proportionality, and it is assumed this is equal to the yield point. This may provide a slightly lower yield point estimate than some other techniques for determining the yield point, such as taking the intersection between this line and the line tangent to the peak of the plastic curve.

2.4 Calculation of the Poisson Ratios

Poisson ratios defined as $v = -d\epsilon_x/d\epsilon_y$ (Bodig and Jayne, 1982) (where ϵ is strain, x is transverse direction and y is axial direction) from the method in section 2.3 the slope of the elastic region of the stress strain curve is known for both the x and y directions. In y this is the Young's Modulus, defined as $E_y = \sigma_y/\epsilon_y$ (where σ is stress) (Bodig and Jayne, 1982) and in the x direction $S_x = \sigma_y/\epsilon_x$ (i.e. the force per unit area applied in the y direction results in a displacement in the y and a different displacement in the x direction related by the Poisson ratio). Therefore $S_x = \sigma_y/\epsilon_x$ and $E_y = \sigma_y/\epsilon_y$ so $-\epsilon_x/\epsilon_y = E_y/S_x$ giving $v_{yx} = -E_y/S_x$

2.5 Determining Elastic Moduli and Poisson ratios for use with the orthotropic assumption

Orthotropic materials have symmetry giving rise to the following equalities (Salenon, 2001):

$$\frac{v_{yx}}{E_y} = \frac{v_{xy}}{E_x}, \qquad \frac{v_{zx}}{E_z} = \frac{v_{xz}}{E_x}, \qquad \frac{v_{yz}}{E_y} = \frac{v_{zy}}{E_z} \tag{1}$$

However from the experiments the equalities presented in equation 1 do not hold. This is probably due to a number of reasons, such as the errors inherent in the method of measurements. In order to ensure these equalities hold (which is necessary for the assumption of wood being an optimization is used to find the values which deviate least from all of the experimental values while still satisfying the equality constraints above. Due to the larger absolute values of some constants (for example E_l) the deviation is considered as normalized against the 95% confidence intervals of the mean values in order to give every variable an even weighting for its accuracy. The optimization uses the above constraints and the following objective function:

$$min \sum \frac{|\delta_i - \gamma_i|}{\theta_i} \qquad i = E_r, E_t, E_l, v_{rt}, v_{tr}, v_{tl}, v_{lt}, v_{lr}, v_{rl} \tag{2}$$

Where δ_i is the experimental value of i, γ_i is the new value and θ_i is the 95% confidence interval of δ_i. This optimization was implemented in a least squares sense using the python algorithm scipy.optimize.fmin_slsqp (Jones et al., 01). It should be noted that setting the 95% confidence intervals as bounds worked for all but one case. The Stiff Outerwood sample when tested under tension fails to converge, due to the inequality constraints being incompatible with any combination within the bounds. This is redeemed by increasing the bound to the 99.9% confidence intervals. An average of Elastic moduli obtained from both compression and tension tests was also undertaken. For the r and t directions the values from the non axial plane for each tension and compression were averaged, whereas for the l direction all measurements were averaged. The Poisson ratios from compression tests were used. The reasons for using these particular values are discussed in section **??**.

2.6 Proportional limit (Yield point) Criteria and ultimate failure

The failure criterion presented by Tsai and Wu (1971) provides a general theory of strength for anisotropic materials, other papers have since used this failure criterion and it has been suggested as an appropriate failure criterion for wood and wood products (Mackenzie-Helnwein et al., 2005a,b). Due to the use and acceptance of the theory in other research along with its treatment of experimental results allowing for pure tension and compression to be regarded separately make it a good choice for investigation into the properties of green wood. The separate treatment of pure tension and compression is needed as wood has

been reported to behave substantially differently under the two regimes (Ozyhar et al., 2013; Bodig and Jayne, 1982). Shear loading is extremely difficult to test within wood due to the material structure being very week in planes perpendicular to the longitudinal axis (i.e. separation between cells requires much less force than breakdown of the cells themselves). The problem of separation is evident in shear tests where the samples are likely to split under the rotational loading (although this loading is assumed to be negligible, it is often significant (Bodig and Jayne, 1982)) between the cells rather than fracture through the desired plane. In the future this could be overcome by using different equipment and more sophisticated shear tests such as those presented in (BS, 1957) or Kollmann and Cote (1968). It has also been suggested that shear properties are best derived from torsion or various bending tests (Moden, 2008).

The full power of Tsai and Wu (1971) failure criterion was not used in this paper. The off axis interaction terms are ignored. The implementation of Tsai and Wu's failure criterion is described in equation 3

$$\boldsymbol{\sigma}^T \boldsymbol{q} + \boldsymbol{\sigma}^T \boldsymbol{P} \boldsymbol{\sigma} - 1 = 0 \tag{3}$$

Where:

$$\boldsymbol{\sigma} = \begin{bmatrix} \sigma_r \\ \sigma_t \\ \sigma_l \\ \sigma_{tl} \\ \sigma_{lr} \\ \sigma_{rt} \end{bmatrix} \tag{4}$$

$$\boldsymbol{q} = \begin{bmatrix} F_{rr} \\ F_{tt} \\ F_{ll} \\ 0 \\ 0 \\ 0 \end{bmatrix} \tag{5}$$

$$\boldsymbol{P} = \begin{bmatrix} F_{rrrr} & F_{rrtt} & F_{rrll} & 0 & 0 & 0 \\ F_{rrtt} & F_{tttt} & F_{ttll} & 0 & 0 & 0 \\ F_{rrll} & F_{ttll} & F_{llll} & 0 & 0 & 0 \\ 0 & 0 & 0 & F_{tltl} & 0 & 0 \\ 0 & 0 & 0 & 0 & F_{lrlr} & 0 \\ 0 & 0 & 0 & 0 & 0 & F_{rtrt} \end{bmatrix} \tag{6}$$

with $\boldsymbol{\sigma}$ as the stress vector, F_{ii}, F_{ij}, F_{iiii} and F_{ijij} described in equations 7 to 10:

$$F_{ii} = \frac{1}{f_{it}} - \frac{1}{f_{ic}} \qquad i = r, t, l \tag{7}$$

$$F_{ij} = \frac{1}{f_{ijt}} - \frac{1}{f_{ijc}} \qquad i, j = r, t, l \;\; (i \neq j) \tag{8}$$

$$F_{iiii} = \frac{1}{f_{it} f_{ic}} \qquad i = r, t, l \tag{9}$$

$$F_{ijij} = \frac{1}{f_{ij}^2} \qquad i, j = r, t, l \;\; (i \neq j) \tag{10}$$

Where f_{it} and f_{ic} are the tensile and compressive strengths in the i direction with f_{ij} the shear strengths. In a simplified case F_{iijj} is ignored giving the following $\boldsymbol{P}$ matrix with no interaction terms:

$$\boldsymbol{P} = \begin{bmatrix} F_{rrrr} & 0 & 0 & 0 & 0 & 0 \\ 0 & F_{tttt} & 0 & 0 & 0 & 0 \\ 0 & 0 & F_{llll} & 0 & 0 & 0 \\ 0 & 0 & 0 & F_{tltl} & 0 & 0 \\ 0 & 0 & 0 & 0 & F_{lrlr} & 0 \\ 0 & 0 & 0 & 0 & 0 & F_{rtrt} \end{bmatrix} \tag{11}$$

The system of equations is solved using optimization techniques. As only two of the six stresses are of interest at any one time (due to visualisation requirements), one is set as the independent variable and a linear space set-up to provide each point that will be evaluated ($n = 1000$), the other four stress directions which are not of interest are set to 0, and the dependent variable is calculated by maximising the distance $\sqrt{\sigma_{independent}^2 + \sigma_{dependent}^2}$ subject to equation 3, completed using the scipy.optimize.fmin_ slsqp algorithm (Jones et al., 01). The proportional limit criterion (assumed to be the same as the yield criterion) is reported in all directions, however the ultimate failure criterion is only reported for the tensile tests. In the tensile direction ultimate failure is characterised by very quick drop in stress to near zero, this happens when the sample breaks into two parts. In the compressive direction ultimate failure is harder to define, if it is considered as the start of sample densification, the experimental results in this study are unable to provide the required information. The tests were limited to a maximum strain of 0.25. Other studies in dry wood have shown densification starts at strains greater than 0.5 (Gibson, 1997). When considering the tree as a living structure it is hard to conserve of a case in nature where densification would occur without ultimate tensile failure occurring on the opposite side of the stem.

3 Results and Discussion

A number of descriptive properties of the samples are presented in Table 2. As is widely reported the outer wood boards were of higher dry density and lower MFA (and in turn faster acoustic velocity) resulting in higher axial dynamic modulus. It is important to note that the variation between the extremes is larger in corewood than between outerwood samples with the stiff corewood sample being of similar properties as the outerwood.

The Elastic moduli and Poisson ratios here were obtained through the optimization and averaging. Table 5 uses Poisson ratios from the compressive

tests, the Elastic moduli from non-longitudinal faces where possible and all four faces for the axial direction. Tension and compression values are averaged and optimised.

Figure 1 shows the failure planes calculated as described above with no interaction terms. The behaviour of the two core wood samples are of interest, while the outer wood samples are stronger in longitudinal tension than compression, the core wood samples are much more centred on the zero axis.

Experimentally obtained values are reported in Table 6. Measurements of the same directional force (eg, lr_t and lt_t could be averaged, as they are both measurements of the same phenomenon.

Table 7 presents multiple measurements of the same tests, reported here as lr and lt, rt and rl, tr and tl. These can be averaged to calculate the three ultimate strengths, but are reported separately for completeness.

The proportional limit surfaces show the propensity for wood to be stronger in the axial tensile direction than any other when considering the high density (outerwood) samples. An interesting phenomenon occurs with decreasing density, the samples become more centred or even favour compression in the longitudinal direction. Both corewood samples indicate the compressive strength is much more important than it is in the outerwood samples (which follow the more traditional idea of higher strength in tension). Some examples that might have an impact on this are the low second moment of area from the thin stem meaning the tree must withstand much more movement from wind, resulting in more compression wood like cells being produced at young ages. Animals stepping on stems causing compressive destruction may have an effect. The trend may also be a by product of a non mechanical pressure. It is possible that because these samples were taken from fully growth trees, (typically 25-30 years old) that over time the material structure has been degraded by growth stresses, or other time/growth dependent phenomenon resulting in a reduction in tensile strength, which is not present if the wood is tested from a young tree.

The Elastic and Shear moduli are low although similar to published values for dry wood, as are the Poisson ratios, as can be seen in Tables 8 and 9. The lower values presented here are not unexpected due to the samples being in green condition and from *Pinus radiata*. In order to accurately quantify the differences between green and dry wood values more accurate testing procedures along with a higher number of samples are needed.

Corewood needs further investigation as this study provides some interesting results, particularly the failure planes in the longitudinal direction. With the corewood samples providing a higher ratio of compressive to tensile strength than outerwood samples. Investigation is needed to determine if this is a property of core wood produced by seedlings and young trees, or if it forms differently and is modified over time while the tree grows. Again to accurately quantify the difference between dry and green wood properties a larger number of more accurate tests are needed.

It should be kept in mind that only four boards were tested during this experiment and those boards were selected as extreme cases of green density and acoustic velocity. The selection criteria and low sample number result in

the selected samples not being representative of the species in general. In order to gain an understanding of the 'average' stem further testing is needed.

This paper did not consider interaction terms within the **P** matrix, Tsai and Wu (1971) suggest the use of experimentation to find the appropriate interaction terms for use within their strength criterion. Further research should not only focus on increasing the size and accuracy of data sets of anisotropic constants but also include these interaction terms to increase the accuracy of further calculation.

References

Apiolaza, L. A., Butterfield, B., Chauhan, S. S., and Walker, J. C. F. (2011). Characterization of mechanically perturbed young stems: Can it be used for wood quality screening? *Annals of Forest Science*, 68(2):407–414.

Barker, J. (1998). The properties of in-grade *Pinus radiata* timber from peeler cores.

Bodig, J. and Jayne, B. A. (1982). *Mechanics of wood and wood composites*. New York: Van Nostrand Reinhold.

BS (1957). *Methods of testing small clear specimens of timber, BS 373:1957*. BSI British Standards.

Cave, I. and Robinson, W. (1998a). Interpretation of (002) diffraction arcs by means of a minimalist model. *Mircofibril Angle in Wood, International Association of Wood Anatomists*, pages 108–115.

Cave, I. and Robinson, W. (1998b). Measuring microfibril angle distribution in the cell wall by means of x-ray diffraction. *Mircofibril Angle in Wood, International Association of Wood Anatomists*, pages 94–107.

Chauhan, S. S., Sharma, M., Thomas, J., Apiolaza, L. A., Collings, D. A., and Walker, J. C. (2013). Methods for the very early selection of *Pinus radiata* D. Don. for solid wood products. *Annals of Forest Science*, 70(4):439–449.

Chris Eberl, Robert Thompson, D. G. S. B. (2006–). Digital image correlation and tracking with matlab.

Contributors, V. (2013). Gphoto2, version 2.5.1.

Downes, G. M., Nyakuengama, J. G., Evans, R., Northway, R., Blakemore, P., Dickson, R. L., and Lausberg, M. (2002). Relationship between wood density, microfibril angle and stiffness in thinned and fertilized *Pinus radiata*. *Iawa Journal*, 23(3):253–265.

Gardiner, B., Byrne, K., Hale, S., Kamimura, K., Mitchell, S. J., Peltola, H., and Ruel, J.-C. (2008). A review of mechanistic modelling of wind damage risk to forests. *Forestry*, 81(3):447–463.

Gibson, L.and Ashby, M. (1997). *Cellular solids: structure and properties*. Cambridge; New York: Cambridge University Press, 2nd edition.

Harrington, J. J. (2002). *Hierarchical modelling of softwood hygro-elastic properties*. Mechanical engineering, University of Canterbury, Christchurch, New Zealand.

Henrik, D. and Gustafsson, P. J. (2013). A three dimensional plasticity model for perpendicular to grain cohesive fracture in wood. *Engineering Fracture Mechanics*, 98:137–152.

Jones, E., Oliphant, T., Peterson, P., et al. (2001–). SciPy: Open source scientific tools for Python.

Kern, K. A., Ewers, F. W., Telewski, F. W., and Koehler, L. (2005). Mechanical perturbation affects conductivity, mechanical properties and aboveground biomass of hybrid poplars. *Tree Physiology*, 25(10):1243–1251.

Kollmann, F. and Cote, W. (1968). *Principles of Wood Science and Technology. Part I Solid Wood*. Springer-Verlag Berlin Heidelberg New York.

Lasserre, J.-P., Mason, E. G., Watt, M. S., and Moore, J. R. (2009). Influence of initial planting spacing and genotype on microfibril angle, wood density, fibre properties and modulus of elasticity in *Pinus radiata D. Don* corewood. *Forest Ecology and Management*, 258(9):1924–1931.

Lindstrm, H., Harris, P., and Nakada, R. (2002). Methods for measuring stiffness of young trees. *Holz als Roh- und Werkstoff*, 60(3):165–174.

Lindstrm, H., Harris, P., Sorensson, C. T., and Evans, R. (2004). Stiffness and wood variation of 3-year old *Pinus radiata* clones. *Wood Science and Technology*, 38(8):579–597.

Lundh, F. et al. (1995–). *Python Imaging Library*.

Mackenzie-Helnwein, P., Eberhardsteiner, J., and Mang, H. A. (2005a). Rate-independent mechanical behavior of biaxially stressed wood: Experimental observations and constitutive modeling as an orthotropic two-surface elasto-plastic material. *Holzforschung*, 59(3):311–321.

Mackenzie-Helnwein, P., Mllner, H. W., Eberhardsteiner, J., and Mang, H. A. (2005b). Analysis of layered wooden shells using an orthotropic elasto-plastic model for multi-axial loading of clear spruce wood. *Computer Methods in Applied Mechanics and Engineering*, 194(21–24):2661–2685.

Moden, C. S. (2008). *Micromechanics of softwoods in the transverse plane: effects on cell and annual ring scales*. PhD thesis, KTH Royal Institute of Technology, Stockholm, Sweden.

Ormarsson, S. and Cown, D. (2005). Moisture-related distortion of timber boards of radiata pine: Comparison with norway spruce. *Wood and Fiber Science*, 37(3):424–436.

Ozyhar, T., Hering, S., and Niemz, P. (2013). Moisture-dependent orthotropic tension-compression asymmetry of wood. *Holzforschung*, 67(4):395–404.

Persson, K. (2000). *Micromechanical Modelling of Wood and Fibre Properties*. Structural mechanics, Lund University, Lund, Sweeden.

Qing, H. and Mishnaevsky, L. (2009). 3D hierarchical computational model of wood as a cellular material with fibril reinforced heterogeneous multiple layers. *Mechanics of Materials*, 41(9):1034–1049.

Raffaele, D. A., Riggio, M., Girardi, G., and Piazza, M. (2011). Morphology-based macro-scale finite-element timber models. *Computer-Aided Design*, 43(1):72–87.

Salenon, J. (2001). *Handbook of continuum mechanics: general concepts, thermoelasticity*. Berlin; New York: Springer.

Skaar, C. (1988). *Wood-Water Relations*. Springer Series in Wood Science. Springer-Verlag.

Tsai, S. W. and Wu, E. M. (1971). General theory of strength for anisotropic materials. *Journal of Composite Materials*, 5:58–80.

Waghorn, M. J., Watt, M. S., and Mason, E. G. (2007). Influence of tree morphology genetics, and initial stand density on outerwood modulus of elasticity of 17-year-old *Pinus radiata*. *Forest Ecology and Management*, 244(1-3):86–92.

Watt, M. S., Clinton, P. W., Coker, G., Davis, M. R., Simcock, R., Parfitt, R. L., and Dando, J. (2008). Modelling the influence of environment and stand characteristics on basic density and modulus of elasticity for young *Pinus radiata* and *Cupressus lusitanica*. *Forest Ecology and Management*, 255(3-4):1023–1033.

Watt, M. S., Moore, J. R., Faon, J.-P., Downes, G. M., Clinton, P. W., Coker, G., Davis, M. R., Simcock, R., Parfitt, R. L., Dando, J., Mason, E., and Bown, H. (2006). Modelling the influence of stand structural, edaphic and climatic influences on juvenile *Pinus radiata* dynamic modulus of elasticity. *Forest Ecology and Management*, 229(1-3):136–144.

Watt, M. S., Sorensson, C., Cown, D. J., Dungey, H. S., and Evans, R. (2010). Determining the main and interactive effect of age and clone on wood density, microfibril angle, and modulus of elasticity for *Pinus radiata*. *Canadian Journal of Forest Research*, 40(8):1550–1557.

Watt, M. S. and Zoric, B. (2010). Development of a model describing modulus of elasticity across environmental and stand density gradients in plantation-grown *Pinus radiata* within New Zealand. *Canadian Journal of Forest Research*, 40(8):1558–1566.

Watt, M. S., Zoric, B., Kimberley, M. O., and Harrington, J. (2011). Influence of stocking on radial and longitudinal variation in modulus of elasticity microfibril angle, and density in a 24-year-old *Pinus radiata* thinning trial. *Canadian Journal of Forest Research*, 41(7):1422–1431.

Xinguo, L., Wu, H. X., and Southerton, S. G. (2011). Transcriptome profiling of *Pinus radiata* juvenile wood with contrasting stiffness identifies putative candidate genes involved in microfibril orientation and cell wall mechanics. *BMC Genomics*, 12(1):480.

Xu, P., Donaldson, L., Walker, J., Evans, R., and Downes, G. (2004). Effects of density and microfibril orientation on the vertical variation of low-stiffness wood in radiata pine butt logs. *Holzforschung*, 58(6):673–677.

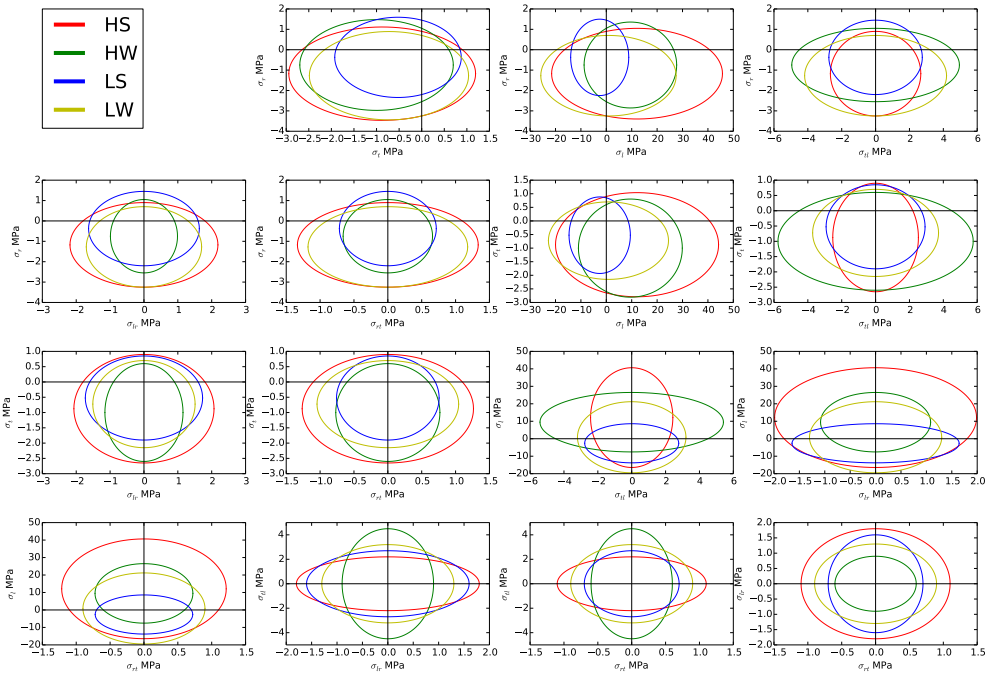

Figure 1: Proportional limit surfaces calculated using Tsai and Wu (1971) failure criterion with no interaction for all failure planes.

Table 1: The four samples shown along with their properties known at the time of selection. Green density was measured using a measuring tape to get an approximate volume and field scales to get the weight of the board. Tree tap was used to get the acoustic velocity. Ring number and wood type from visual inspection

Sample	Green Density	Acoustic velocity	Approximate ring number	Type of wood
Stiff Outerwood	high	high	> 15	Sapwood
Non-Stiff Outerwood	high	low	> 15	Sapwood
Stiff Corewood	low	high	< 15	Heartwood
Non-Stiff Corewood	low	low	< 15	Heartwood

Table 2: Table showing the wood properties of the samples. Densities are averages from measuring all of the specimens individually. Disk scanner velocities are averages from individual specimens or a block of no more than six specimens depending on the size and shape. Wood spec velocities are from sections of board 500 mm in length, which were not used for specimens, taken in wet condition. MFA is obtained from x-ray diffraction after testing and drying.

Property	Stiff Outerwood	Non-Stiff Outerwood	Stiff Corewood	Non-Stiff Corewood
Green Density, kg/m^3	1143 (3)	1099 (9)	933 (21)	818 (22)
Dry Density, kg/m^3	531 (5)	458 (9)	438 (8)	393 (5)
Acoustic Velocity m/s Disk Scanner (green)	4651 (8)	4221 (26)	4191 (34)	3413 (14)
Acoustic Velocity m/s Wood Spec (green)	3490	3470	3470	2700
Wood Type	outerwood	outerwood	corewood?	corewood
Ring Number	> 15	> 15	< 15	< 15
MFA, *Degrees*	7	8	9	21
Standard Deviation of MFA *Degrees*	9	12	11	12

Table 3: Young's Moduli obtained from various UTM tests. The first letter is the direction of force, the second, the face which was recorded and the third t is a tension force and c is a compressive force. Capital letters indicate the shear moduli in the given plane.

Direction	Stiff Outerwood		Non-Stiff Outerwood		Stiff Corewood		Non-Stiff Co
	E	SE	E	SE	E	SE	E
rt_t in GPa	0.40	0.11	0.24	0.05	0.13	0.01	0.16
rt_c in GPa	0.58	0.08	0.36	0.10	0.39	0.03	0.47
rl_t in GPa	0.62	0.10	0.13	0.04	0.37	0.11	0.12
rl_c in GPa	0.57	0.07	0.58	0.09	0.45	0.07	0.54
tr_t in GPa	0.13	0.01	0.22	0.04	0.20	0.02	0.09
tr_c in GPa	0.33	0.03	0.35	0.07	0.29	0.07	0.26
tl_t in GPa	0.30	0.11	0.08	0.01	0.14	0.01	0.14
tl_c in GPa	0.37	0.04	0.36	0.03	0.22	0.02	0.29
lr_t in GPa	10.74	1.83	3.78	0.93	3.03	0.90	4.33
lr_c in GPa	3.10	0.11	1.02	0.50	3.76	0.80	4.04
lt_t in GPa	11.74	2.18	4.69	1.13	3.23	1.50	4.05
lt_c in GPa	7.47	1.60	1.74	0.61	4.65	1.06	5.85
TL in MPa	111.7	7.3	211.1	3.9	107.0	1.2	125.8
LR in MPa	59.7	1.9	34.4	1.2	38.5	1.7	29.5
RT in MPa	45.9	1.3	22.8	1.7	22.5	1.4	39.0

Table 4: v is the Poisson ratio and SE is the standard error on the ratio. First letter is the direction of force, the second the face which was recorded and the third t is a tension force and c is a compressive force.

Direction	Stiff Outerwood		Non-Stiff Outerwood		Stiff Corewood		Non-Stiff Corew
	v	SE	v	SE	v	SE	v
rt_t	0.21	0.10	0.30	0.08	0.27	0.12	0.08
rt_c	0.64	0.04	0.52	0.09	0.60	0.05	0.49
rl_t	0.26	0.08	0.04	0.02	0.31	0.15	0.15
rl_c	0.14	0.04	0.15	0.05	0.22	0.14	0.17
tr_t	0.20	0.03	0.19	0.05	0.53	0.22	0.02
tr_c	0.47	0.10	0.33	0.04	0.39	0.08	0.42
tl_t	0.15	0.05	0.09	0.03	0.04	0.02	0.62
tl_c	0.10	0.02	0.08	0.04	0.18	0.08	0.08
lr_t	0.24	0.08	0.42	0.18	0.30	0.01	0.35
lr_c	0.26	0.05	0.41	0.13	0.36	0.08	0.44
lt_t	0.48	0.14	0.29	0.10	0.39	0.17	0.21
lt_c	0.41	0.08	0.16	0.06	0.37	0.09	0.42

Table 5: Optimized values for the orthotropic assumption. All Poisson ratios used are from compression teststhe moduli are reported calculated from averages of tension and compression. In the r and t directions this is the average of tension and compression from the camera viewing the rt or tr plane. In the longitudinal direction it is the average of all four image sets.

Average Direction	Stiff Outerwood	Non-Stiff Outerwood	Stiff Corewood	Non-Stiff Corewood
E_r	0.49	0.30	0.26	0.31
E_t	0.25	0.19	0.24	0.17
E_l	4.36	2.81	3.50	2.38
v_{rt}	0.64	0.54	0.60	0.77
v_{rl}	0.03	0.05	0.03	0.06
v_{tr}	0.33	0.33	0.55	0.42
v_{tl}	0.03	0.01	0.03	0.04
v_{lr}	0.29	0.47	0.36	0.44
v_{lt}	0.60	0.16	0.37	0.50

Table 6: Proportional limit values in MPa the first letter is the direction of force, the second the face which was recorded and the third t is a tension force and c is a compressive force. Capital letters are the planes of shear.

Direction	Stiff Outerwood		Non-Stiff Outerwood		Stiff Corewood		Non-Stiff Corewoo
	S	SE	S	SE	S	SE	S
rt_t	0.8	0.2	1.3	0.5	1.2	0.3	0.9
rt_c	-3.2	0.1	-2.5	0.2	-2.1	0.1	-3.2
rl_t	1.0	0.1	0.8	0.2	1.7	0.4	0.5
rl_c	-3.3	0.2	-2.6	0.1	-2.3	0.1	-3.3
tr_t	0.8	0.2	0.7	0.2	0.9	0.1	0.6
tr_c	-2.7	0.1	-2.4	0.3	-1.8	0.2	-2.0
tl_t	1.0	0.3	0.5	0.1	0.8	0.2	0.8
tl_c	-2.6	0.2	-2.8	0.2	-2.0	0.1	-2.3
lr_t	46.0	7.5	26.0	1.3	7.6	1.8	21.8
lr_c	-17.4	1.0	-6.6	2.9	-14.0	1.1	-17.6
lt_t	35.3	3.8	27.0	4.5	9.6	2.4	20.6
lt_c	-15.5	1.5	-8.5	3.5	-13.6	1.6	-21.4
TL	2.2	0.4	4.5	0.3	2.7	0.2	3.2
LR	1.8	0.1	0.9	0.2	1.6	0.3	1.3
RT	1.1	0.2	0.6	0.2	0.7	0.1	0.9

Table 7: Ultimate strength reported in MPa. Only tensile strength is reported, the first letter is the direction of the force, second is the plane of imaging.

Direction	Stiff Outerwood		Non-Stiff Outerwood		Stiff Corewood		Non-Stiff Corewoo
	S	SE	S	SE	S	SE	S
rt	3.1	0.3	3.1	0.3	2.9	0.2	2.2
rl	3.1	0.3	3.0	0.3	2.8	0.3	2.2
tr	2.1	0.4	1.6	0.3	1.9	0.1	2.1
tl	2.1	0.5	1.4	0.3	1.9	0.1	2.1
lr	64.2	5.9	45.2	4.6	21.2	1.6	32.6
lt	65.0	5.7	43.6	5.1	20.0	1.9	32.8

Table 8: Comparison of literature values with the findings in this study. Values are aproximate as a number of them were taken from published plots. All Moduli in GPa.

Reference	Test	Species	E_r	E_t	E_l	G_{tl}	G_{lr}	G_{rt}	v_{rt}	v_{rl}	v_{tr}	v_{tl}	v_{lr}	v_{lt}
This work	Static	*Pinus radiata*	0.26	0.17	2.38	0.11	0.03	0.02	0.54	0.03	0.33	0.01	0.29	0.16
(Range)			0.49	0.25	4.36	0.21	0.06	0.05	0.77	0.06	0.55	0.04	0.47	0.60
Ozyhar et al. (2013)	Static	*Fagus sylvatica*	1.14	0.53	9.14				0.19	0.39	0.47	0.5	0.04	0.03
(Range)			2.33	1.05	14.54				0.41	0.55	0.76	0.87	0.2	0.11
Henrik and Gustafsson (2013)			0.8	0.5	12	0.7	0.7	0.05		0.02	0.3	0.02		
Raffaele et al. (2011)	Hybrid	*Picea Abies*	0.236	0.387	10.4	0.65	0.597	0.029	0.42	0.018		0.017		
Mackenzie-Helnwein et al. (2005a)	Hybrid	Spruce	0.7	0.5	13	0.47	0.63	0.22	0.38			0.013	0.5	
Ormarsson and Cown (2005)	Hybrid	*Pinus radiata*	0.7	0.2	5	0.6	1	0.05						
(Range)			2.2	0.7	19	1.2	2	0.15						
Qing and Mishnaevsky (2009)	Theoretical			2.202	20.25	1.94		1.4						
Harrington (2002)	Theoretical	*Pinus radiata*	0.56	0.23	5.61	1.0	1.20	0.08		0.42	0.38	0.37		
(Range)			3.08	3.08	9.33	2.18	2.07	0.79		0.48	1.23	0.45		
Persson (2000)	Theoretical	Spruce	0.67	0.08	7.7	0.40	0.68	0.009		0.009	0.124	0.006		
(Range)			1.57	2.1	36.4	1.77	1.76	0.043		0.057	0.241	0.054		

Table 9: Literature values for the longitudinal elastic moduli. Values are aproximate as a number of them were taken from published plots. All moduli in GPa.

Reference	Test	Species	E_l
Watt et al. (2006)	Dynamic	*Pinus radiata*	2 - 7
Waghorn et al. (2007)	Dynamic		5 - 9
Lindstrm et al. (2004)	Dynamic		2 - 4.8
Xinguo et al. (2011)	Dynamic		3 - 6
Watt et al. (2008)	Dynamic		2.4 - 5.9
Lasserre et al. (2009)	Dynamic		2.7 - 4.2
Watt et al. (2011)	Silviscan		3 - 15
Downes et al. (2002)	Silviscan		11.5 - 13.5
Watt et al. (2010)	Silviscan		1.4 - 21.6
Watt and Zoric (2010)	Silviscan		3 - 18
Xu et al. (2004)	Static		4.8 - 14.9
Lindstrm et al. (2002)	Static		2.5 - 6